HHS Public Access

Author manuscript

Spine J. Author manuscript; available in PMC 2017 April 01.

Published in final edited form as:

Spine J. 2016 April ; 16(4): 540–546. doi:10.1016/j.spinee.2015.11.052.

Dimensional Changes of the Neuroforamen in Sub-axial Cervical Spine during *In Vivo* Dynamic Flexion-Extension

Haiqing Mao, MD[*,†], **Sean J Driscoll, MEng**[*], **Jing-Sheng Li, MS**[*], **Guoan Li, PhD**[*], **Kirkham B Wood, MD**[*], and **Thomas D Cha, MD, MBA**[*]

[*]Bioengineering Laboratory, Department of Orthopedic Surgery, Harvard Medical School / Massachusetts General Hospital, Boston, MA

[†]Department of Orthopedic Surgery, the First Affiliated Hospital of Soochow University, Suzhou, Jiangsu, China

Abstract

Background Context—Neuroforaminal stenosis is one of the key factors causing clinical symptoms in patients with cervical radiculopathy. Previous quantitative studies on the neuroforaminal dimensions have focused on measurements in a static position. Little is known about dimensional changes of the neuroforamen in the cervical spine during functional dynamic neck motion under physiological loading conditions.

Purpose—To investigate the *in vivo* dimensional changes of the neuroforamen in human cervical spine (C3-C7) during dynamic flexion-extension neck motion.

Study Design—A case-control study.

Methods—10 asymptomatic subjects were recruited for this study. The cervical spine of each subject underwent magnetic resonance image (MRI) scanning for construction of three dimensional (3D) vertebrae models from C3 to C7. The cervical spine was then imaged using a dual fluoroscopic system while the subject performed a dynamic flexion-extension neck motion in a sitting position. The 3D vertebral models and the fluoroscopic images were used to reproduce the *in vivo* vertebral motion. The dimensions (area, height and width) were measured for each cervical neuroforamen (C3/C4, C4/C5, C5/C6 and C6/C7) in the following functional positons: neutral positon, maximal flexion and maximal extension. Repeated measures ANOVA and post-hoc analysis were used to examine the differences between levels and positions.

Results—Compared with the neutral position, almost all dimensional parameters (area, height and width) of the sub-axial cervical neuroforamen decreased in extension and increased in flexion,

Corresponding author: Guoan Li, PhD, Orthopedic Bioengineering Laboratory, Harvard Medical School/Massachusetts General Hospital, 55 Fruit Street - GRJ 1215, Boston, MA 02114, USA, Tel: +1-617-726-6472 Fax: +1-617-724-4392, gli1@partners.org.

Conflict of interest: None.

Statement of IRB Approval: This research was approved by the Partners Human Research Committee (Protocol Number: 2012P002508/MGH).

except the neuroforaminal area at C5/C6 (P=0.07) and the neuroforaminal height at C6/C7 (P=0.05) remained relatively constant from neutral to extension. When comparisons of the overall change from extension to flexion were made between segments, the overall changes of the neuroforaminal area and height revealed no significant differences between segments, the width overall change of the upper levels (C3/C4 and C4/C5) was significantly greater than the lower levels (C5/C6 and C6/C7) (P<0.01).

Conclusions—The dimensional changes of the cervical neuroforamen showed segment-dependent characteristics during the dynamic flexion-extension. These data may have implications for diagnosis and treatment of patients with cervical radiculopathy.

Keywords

Neuroforaminal dimension; Kinematics; Cervical spine; Fluoroscopy

Introduction

Although the pathophysiology of cervical radiculopathy is not completely understood, mechanical compression of nerve roots combined with inflammatory changes is often thought of the key factor leading to pain and neurologic dysfunction [1]. The cervical neuroforaminal zone is the most common region associated with nerve roots impingement as degenerative changes such as disc herniation and osteophyte formation can lead to neuroforaminal stenosis [2, 3]. Clinically, symptoms associated with radiculopathy may be intensified by cervical extension, and relived by cervical flexion [4]. It is therefore believed that changes in dimensions of the neuroforamen during neck motion could cause impingement of the nerve root within the cervical neuroforamen in patients with cervical radiculopathy. Therefore, understanding the geometric characters of the neuroforamen is critical to the understanding of the pathophysiology of cervical radiculopathy.

Many *in vitro* studies have reported significant decreases in neuroforamen dimensions from flexion to extension of the neck using cervical cadaveric specimens [5-7]. *In vivo* studies have also indicated position-dependent changes of the neuroforaminal dimensions at different flexion-extension postures using oblique radiographs, sagittal reconstructed computed tomography (CT) images [8] and magnetic resonance imaging (MRI) [9]. While these studies have greatly improved our knowledge of cervical neuroforaminal dimensions, most of the data were obtained from static measurements using standard modalities of radiograph, CT and MRI. Furthermore, in these studies, the subjects usually are not in an upright weight bearing position during the CT and MRI scanning. Therefore, the dynamic changes of the neuroforaminal dimensions under physiological loading conditions remain unclear. Few data has been reported on the differences in neuroforaminal changes at segment levels.

Recently, model-based three dimensional (3D) imaging techniques via high-speed biplane radiography have been developed for non-invasive measurements of 3D, dynamic intervertebral kinematics of the cervical spine during functional neck flexion and extension [10-13]. This technique makes it possible to determine dynamic dimensional changes of the neuroforamen in the sub-axial cervical spine. Therefore, the objective of this study was to

quantitatively determine the changes of area, height, and width of the cervical neuroforamen using a validated 3D dual fluoroscopic imaging technique [14]. Specifically, we compared the neuroforaminal dimensions at different segment levels during dynamic neck flexion-extension motion of living human subjects.

Materials and Methods

Study populations

Ten asymptomatic subjects (6 males, 4 females, average age: 40.3±10.9 years, average BMI 24.6±3.2 kg/m^2) were recruited from a single academic center. The presence of any spinal disorders, symptoms, or anatomic abnormalities were used as exclusion factors from the study. Approval by our institutional review board was obtained prior to the initiation of this study. Informed consent was obtained from each patient before any testing was performed.

Dual fluoroscopic imaging technique

The cervical spine of each subject underwent an MRI scan using a 3 Tesla scanner (MAGNETOM Trio, Siemens, Germany) with a spine surface coil and a proton density weighted sequence. The subject was scanned in a supine, relaxed position. Parallel digital images with a voxel size of 0.625 × 0.625 × 1.500 mm^3 and a resolution of 282 × 384 pixels were obtained. The MR images were then imported into solid modeling software (3D Slicer) [15] to construct 3D models of the C3, C4, C5, C6 and C7 vertebrae.

Following MRI scanning, the cervical spines of the subjects were imaged using a dual orthogonal fluoroscopic system. Two fluoroscopes (BV Pulsera, Phillips, Bothell, WA) were positioned with their image intensifiers perpendicular to each other in order to capture images of the segments at different postures from two orthogonal directions simultaneously. The subjects were asked to sit on a chair with the trunk stabilized and position their cervical spines within the views of the two fluoroscopes. After the images of the cervical spine in a static neutral position were obtained, the kinematics of C3-C7 were captured as the subjects performed a neck flexion-extension motion. The fluoroscopes captured the dynamic spinal positions at 30 frames per second with an 8 ms pulse. During fluoroscopic imaging, the subject was protected by lead skirts and vests below their cervical spines to minimize radiation exposure.

The geometry of the dual fluoroscopic system was recreated in solid modeling software (Rhinoceros, Robert McNeel & Associates, Seattle, WA). After calibration, the pair of the fluoroscopic images were imported into the software and placed in virtual orthogonal planes to simulate the positions of the intensifiers. The 3D models of the cervical vertebrae were introduced into the virtual system and were independently translated and rotated in 6DOF, until their silhouettes matched those captured on the two orthogonal fluoroscopic images. Thus, the *in vivo* positions of the cervical vertebrae along the dynamic flexion-extension motion path were reproduced. The mean accuracy of our image-matching technique in determining intervertebral kinematics has been shown to be less than 0.4mm, and the repeatability was less than 0.3 mm in translation and less than 0.7° in orientation [14].

Measurements of the cervical neuroforamen

The neuroforamen of the cervical spine is bounded superiorly and inferiorly by the pedicles of the adjacent vertebrae. In the solid modeling software (Rhinoceros), we subdivided the sub-axial cervical spine into four segment levels: C3/C4, C4/C5, C5/C6 and C6/C7. For each segment level, we adjusted the viewing angle until the upper and lower pedicles on one side of the neuroforamen were superimposed representing a true “axial” view of the foramen between the two vertebrae of interest. The actual spatial relationships of the two vertebrae at each segment level remained unchanged in the process of viewing adjustment.

The central line along the long axis of ipsilateral upper and lower pedicles was then defined at the plane on which both pedicles overlapped completely. We cut the pedicles along the central line perpendicular to this plane using Section tool in the software. The oblique sagittal plane passing through the long axis of both pedicles which composed the neuroforamen was then set up (Figure 1). The border of the neuroforamen were formed by the inferior edge of the upper pedicle, the posterior uncovertebral joint, the superior edge of the lower pedicle, the anterior margin of the pars interarticularis and the superior articular process.

The neuroforaminal dimensions of each segment were measured in the neutral, full flexion and full extension positions along the dynamic motion path (Figure2). Dimensional parameters included the neuroforaminal area, the neuroforaminal height and the neuroforaminal width. The neuroforaminal area was calculated according to the neuroforaminal bony outline. The neuroforaminal height was defined as the longest distance between the borders of the upper and lower pedicles. The neuroforaminal width was defined as the shortest distance between the posterior-inferior corner of the upper vertebra and the anterior border of the superior articular process of the lower vertebra. The neuroforaminal dimensions of each segment were averaged from both sides of the neuroforamen.

Statistical analysis

After acquiring the geometrical parameters of each segment level in different positions, the changes of neuroforaminal area, height and width at flexion and extension positions were calculated with the data at the neutral position as references. The overall changes of the neuroforaminal area, height and width were calculated using the data at flexion to minus the data at extension positions. A repeated-measures analysis of variance (ANOVA) was used to compare the neuroforaminal area, the neuroforaminal height, and the neuroforaminal width of C3/C4, C4/C5, C5/C6 and C6/C7 in the following functional positions: neutral positon, full flexion, and full extension. The level of significance was set at $P < 0.05$. When a significant difference was detected, a Newman-Keuls post hoc test was performed. The statistical analysis was performed using Statistica software (StatSoft, Tulsa, Oklahoma).

Results

Neuroforaminal Area

In the neutral position, the neuroforaminal area at C3/C4, C4/C5, C5/C6 and C6/C7 was $50.1\pm7.5mm^2$, $51.4\pm12.3mm^2$, $48.6\pm10.7mm^2$ and $53.1\pm7.7mm^2$, respectively. Compared

with the neutral position, the neuroforaminal area at C3/C4, C4/C5, C5/C6 and C6/C7 decreased by 4.5mm^2 (9%, P=0.045), 6.0mm^2 (12%, P<0.001), 3.8mm^2 (8%, P=0.068) and 3.9mm^2 (7%, P=0.022) in extension, and increased by 9.1mm^2 (18%, P<0.001), 9.9mm^2 (19%, P<0.001), 4.8mm^2 (10%,P=0.022) and 6.2mm^2 (12%, P<0.001) in flexion (Figure 3). In the same position, there were no significant differences in the neuroforaminal area between segment levels. C4/C5 had the greatest overall area change (31%), followed subsequently by C3/C4 (27%), C6/C7 (19%), and C5/C6 (18%) during flexion-extension (Figure 4). The overall area changes between segments were not significantly different between the segment levels (P=0.169).

Neuroforaminal Height

In the neutral position, the neuroforaminal height at C3/C4, C4/C5, C5/C6 and C6/C7 was 9.5±1.0mm, 9.6±1.5mm, 9.3±1.4mm and 9.7±1.2mm, respectively. From the neutral position to extension, the neuroforaminal height at C3/C4, C4/C5, C5/C6 and C6/C7 decreased by 0.7mm (7%, P=0.003), 1.1mm (11%, P<0.001), 0.6mm (6%, P=0.006) and 0.6mm (6%, P=0.052). From the neutral position to flexion, the neuroforaminal height at C3/C4, C4/C5, C5/C6 and C6/C7 increased by 1.6mm (17%, P<0.001), 1.4mm (15%, P<0.001), 0.9mm (10%, P<0.001) and 1.2mm (12%, P<0.001) (Figure 5). From extension to flexion, C4/C5 had the greatest overall height change (26%), followed subsequently by C3/C4 (24%), C6/C7 (18%), and C5/C6 (16%). The overall height changes between segments were no significantly different (P=0.135) (Figure 6).

Neuroforaminal Width

In the neutral position, the neuroforaminal width at C3/C4, C4/C5, C5/C6 and C6/C7 was 6.3±0.5mm, 6.3±0.6mm, 6.2±0.5mm and 6.6±0.4 mm, respectively. From the neutral position to extension, the neuroforaminal width at C3/C4, C4/C5, C5/C6 and C6/C7 decreased by 0.7mm (11%, P<0.001), 0.8mm (13%, P<0.001), 0.5mm (8%, P<0.001) and 0.5mm (8%, P<0.001). From the neutral position to flexion, the neuroforaminal width at C3/C4, C4/C5, C5/C6 and C6/C7 increased by 1.1mm (17%, P<0.001), 1.4mm (22%, P<0.001), 0.6mm (10%, P<0.001) and 0.7mm (11%, P<0.001) (Figure 7). There were significant differences in the overall width changes among segment levels during the flexion-extension neck motion (P<0.001). The overall width changes at C3/C4 (28%) and C4/C5 (35%) were significantly greater than at C5/C6 (18%) and C6/C7 (19%) (Figure 8).

Discussion

Accurate knowledge of changes of the cervical neuroforaminal geometry is important for elucidating the dynamic factors causing cervical radiculopathy. In this study, we used 3D model-based matching technique to investigate the geometric parameters of the cervical neuroforamen during neck flexion-extension under physiological weight bearing conditions. Our data showed, in general, almost all geometric parameters of the sub-axial cervical neuroforamen decreased from neutral to extension, increased from neutral to flexion positions, except the neuroforaminal area at C5/C6 and the neuroforaminal height at C6/C7 remained relatively constant from the neutral position to extension. In comparisons of the overall change from extension to flexion between segment levels, the overall changes of the

neuroforaminal area and height had no significant differences between segment levels, but the overall change of the neuroforaminal width of the upper levels (C3/C4 and C4/C5) was significantly greater than the lower levels (C5/C6 and C6/C7).

Our study demonstrated the neuroforaminal dimensions in the cervical spine had a reduced tendency from the neutral position to extension and an increased tendency from the neutral position to flexion during the *in vivo* dynamic neck motion under weight-bearing conditions. This tendency was similar to published results measured from *in vitro* cadaveric analyses and *in vivo* imaging studies. Yoo et al [7] reported that the foraminal diameter increased by 10% and decreased by 13% respectively at 30° of flexion and extension as cadaver cervical spines moved under an axial load. The work by Nuckley et al [6] illustrated similar results in another *in vitro* study. Muhle et al [9] used MRI to study changes of the cervical neuroforaminal size in 30 healthy volunteers when subjects were lying on the table. They found the foraminal area was increased by 31% at 40° of flexion, decreased by 20% at 30° of extension compared with the neutral position. Kitagawa et al [8] reported the foraminal area increased by 28% from neutral to flexion, and decreased by 17% from neutral to extension by using reformatted CT images to evaluate 7 healthy subjects. In our study, the average neuroforaminal area changed with 15% of increase at flexion and 9% of decrease at extension.

Although previous studies have shown similar trends in neuroforaminal dimensional changes as our study, the magnitude of dimensional changes were not consistent between these studies. The main factors contributed to this discrepancy were different research subjects and their movement modalities in these studies, including passive movement of cadavers under an axial load, static posture of living subjects in a supine position, and free movement of living subjects in a sitting position. The latter was obviously closer to physiological movement of human body. In our study, the subjects were asked to perform a neck maximal flexion and extension motion actively, that was different from the static postures reported in literature [6, 7, 9]. Another important factor was various technologies for data collection used in these studies, such as X-ray, CT, MRI and 3D matching technique. It should be noted that we reconstructed the 3D models of the sub-axial cervical spine and accurately defined the cross section of each neuroforaminal area. This method was different from sagittal view or oblique view of traditional imaging technique [16-18] which assessed all the cervical neuroforamen in the same angle. We acquired the individual oblique reconstruction image for each cervical neuroforamen by superimposing the upper and lower pedicles composing the neuroforamen, to identify variations between different segments and positions and represent the actual foraminal view.

The present study showed that the dimensional changes of the neuroforamen were segment-dependent. Compared with the lower levels (C5/C6 and C6/C7) of the sub-axial cervical spine, the upper levels (C3/C4 and C4/C5) had similar overall height change but higher overall width change of the neuroforamen. This geometric phenomenon may be associated with intervertebral kinematics and the motion path of the instant center of rotation (ICR) in the cervical spine. Another study using the same subjects of this study showed C3/C4 and C4/C5 had greater the anterior-posterior (AP) movement (4.8mm, 4.8mm, respectively) than C5/C6 and C6/C7 (3.7mm, 2.4mm, respectively) during neck flexion-extension, but the

superior-inferior (SI) movement of all segment levels was similar (1.7-1.8mm) [19]. During *in vivo* dynamic flexion-extension, the ICRs of all sub-axial cervical spinal segments were shown to locate anteriorly to the posterior edges of the vertebral bodies [20, 21]. Anderst et al [21] found that the range of the ICR motion in the SI direction was lower than that in AP direction, and the range of the ICR motion in the AP direction at C3/C4 and C4/C5 was greater than that at C5/C6 and C6/C7. If the rotation angles of different segments were similar, more horizontal translation of ICR in a specific segment may lead to higher overall change of the neuroforaminal width in this segment.

The neuroforaminal stenosis for patients with cervical radiculopathy is usually evaluated clinically using MRI images from the patients in the supine position. These imaging data are useful for analyzing the static compression of nerve roots, but might not accurately reflect the dynamic relationship between neuroforamen and nerve roots during neck motion. When degenerative changes decrease the neuroforaminal height due to disc dessication and narrow the neuroforaminal width due to herniated disc and osteophyte formation, this will reduce the neuroforaminal space available for the nerve roots during extension of the cervical spine. Therefore, detection and assessment of dynamic impingement of the nerve root caused by dimensional changes of the neuroforamen become a key factor for accurate diagnosis and effective treatment of cervical radiculopathy. Furthermore, because the extent of dimensional changes varies from segment to segment, neck motion can bring varying effect on nerve compression at different segment levels even if magnitude of neuroforaminal stenosis is similar. Thus, individual treatment protocols should be made according to the pathological levels and degrees.

Several limitations to this study should be considered. First, the analysis of the cervical spinal neuroforamen was limited to the sub-axial cervical spine. The neuroforamen of C1/C2 and C2/C3 was not included because of the obstruction of the images of the C1 and C2 vertebrae by the mandibular and occipital bones in certain postures along the flexion-extension motion path. Second, we used 3D vertebral models without soft tissues due to the difficulties of specifying soft tissue boundaries around the neuroforamen area. So the effect of ligament folding and disc bulging on the neuroforaminal dimensions was not included in the neuroforaminal measurements. Finally, we only investigated 10 asymptomatic subjects with an age range of 30–59 years. Future studies should recruit more normal and symptomatic patients with cervical spondylosis to clarify the effects of age and degenerative change on the dimensions of the cervical neuroforamen.

In summary, this study investigated the changes of dimensional parameters of the neuroforamen in the sub-axial cervical spine during dynamic a flexion-extension motion of the neck. The upper levels of the sub-axial cervical spine had larger changes in neuroforaminal dimensions than the lower levels during the dynamic neck flexion-extension motion, especially on the overall width change of the neuroforamen. These data may be instrumental for improved understanding of physiological and pathological mechanism of cervical radiculopathy, thus provide implications for improvement of diagnoses and treatments of cervical radiculopathy.

Acknowledgments

The authors would like to gratefully acknowledge financial support from the National Institutes of Health (R21AR057989), K2M Group Holdings, Inc. and Jiangsu Government Scholarship for Overseas Studies (JS-2012-117).

References

1. Garfin SR, Rydevik B, Lind B, Massie J. Spinal nerve root compression. Spine. 1995; 20(16):1810–20. [PubMed: 7502139]
2. Ebraheim NA, An HS, Xu R, Ahmad M, Yeasting RA. The quantitative anatomy of the cervical nerve root groove and the intervertebral foramen. Spine. 1996; 21(14):1619–23. [PubMed: 8839462]
3. Humphreys SC, Hodges SD, Patwardhan A, Eck JC, Covington LA, Sartori M. The natural history of the cervical foramen in symptomatic and asymptomatic individuals aged 20-60 years as measured by magnetic resonance imaging. A descriptive approach. Spine. 1998; 23(20):2180–4. [PubMed: 9802158]
4. Muhle C, Bischoff L, Weinert D, et al. Exacerbated pain in cervical radiculopathy at axial rotation, flexion, extension, and coupled motions of the cervical spine: evaluation by kinematic magnetic resonance imaging. Invest Radiol. 1998; 33(5):279–88. [PubMed: 9609487]
5. Farmer JC, Wisneski RJ. Cervical spine nerve root compression. An analysis of neuroforaminal pressures with varying head and arm positions. Spine. 1994; 19(16):1850–5. [PubMed: 7973984]
6. Nuckley DJ, Konodi MA, Raynak GC, Ching RP, Mirza SK. Neural space integrity of the lower cervical spine: effect of normal range of motion. Spine. 2002; 27(6):587–95. [PubMed: 11884906]
7. Yoo JU, Zou D, Edwards WT, Bayley J, Yuan HA. Effect of cervical spine motion on the neuroforaminal dimensions of human cervical spine. Spine. 1992; 17(10):1131–6. [PubMed: 1440000]
8. Kitagawa T, Fujiwara A, Kobayashi N, Saiki K, Tamai K, Saotome K. Morphologic changes in the cervical neural foramen due to flexion and extension: in vivo imaging study. Spine. 2004; 29(24): 2821–5. [PubMed: 15599285]
9. Muhle C, Resnick D, Ahn JM, Sudmeyer M, Heller M. In vivo changes in the neuroforaminal size at flexion-extension and axial rotation of the cervical spine in healthy persons examined using kinematic magnetic resonance imaging. Spine. 2001; 26(13):E287–93. [PubMed: 11458168]
10. McDonald CP, Bachison CC, Chang V, Bartol SW, Bey MJ. Three-dimensional dynamic in vivo motion of the cervical spine: assessment of measurement accuracy and preliminary findings. The spine journal : official journal of the North American Spine Society. 2010; 10(6):497–504. [PubMed: 20359957]
11. Anderst WJ, Baillargeon E, Donaldson WF 3rd, Lee JY, Kang JD. Validation of a noninvasive technique to precisely measure in vivo three-dimensional cervical spine movement. Spine. 2011; 36(6):E393–400. [PubMed: 21372650]
12. Haque MA, Anderst W, Tashman S, Marai GE. Hierarchical model-based tracking of cervical vertebrae from dynamic biplane radiographs. Medical engineering & physics. 2013; 35(7):994–1004. [PubMed: 23122602]
13. Lin CC, Lu TW, Wang TM, Hsu CY, Hsu SJ, Shih TF. In vivo three-dimensional intervertebral kinematics of the subaxial cervical spine during seated axial rotation and lateral bending via a fluoroscopy-to-CT registration approach. Journal of biomechanics. 2014; 47(13):3310–7. [PubMed: 25218506]
14. Wang S, Passias P, Li G, Li G, Wood K. Measurement of vertebral kinematics using noninvasive image matching method-validation and application. Spine. 2008; 33(11):E355–61. [PubMed: 18469683]
15. Fedorov A, Beichel R, Kalpathy-Cramer J, et al. 3D Slicer as an image computing platform for the Quantitative Imaging Network. Magnetic resonance imaging. 2012; 30(9):1323–41. [PubMed: 22770690]

16. Simpson AK, Sabino J, Whang P, Emerson JW, Grauer JN. The assessment of cervical foramina with oblique radiographs: the effect of film angle on foraminal area. Journal of spinal disorders & techniques. 2009; 22(1):21–5. [PubMed: 19190430]

17. Miller CP, Sabino J, Bible JE, Whang PG, Grauer JN. Oblique radiographs compared favorably with computed tomography images in assessing cervical foraminal area. Am J Orthop (Belle Mead NJ). 2011; 40(5):241–5. [PubMed: 21734932]

18. Park MS, Moon SH, Lee HM, et al. Diagnostic value of oblique magnetic resonance images for evaluating cervical foraminal stenosis. The spine journal : official journal of the North American Spine Society. 2015; 15(4):607–11. [PubMed: 25452016]

19. Cha, TD.; Driscoll, SJ.; Wang, S., et al. Development of a Non-invasive Dual-fluoroscopic Imaging System for Measuring In-vivo Cervical Spine Motion 81st Annual Meeting of the. American Academy of Orthopaedic Surgeons; New Orleans, LA: 2014.

20. Liu B, Liu Z, VanHoof T, Kalala J, Zeng Z, Lin X. Kinematic study of the relation between the instantaneous center of rotation and degenerative changes in the cervical intervertebral disc. European spine journal : official publication of the European Spine Society, the European Spinal Deformity Society, and the European Section of the Cervical Spine Research Society. 2014; 23(11):2307–13.

21. Anderst W, Baillargeon E, Donaldson W, Lee J, Kang J. Motion path of the instant center of rotation in the cervical spine during in vivo dynamic flexion-extension: implications for artificial disc design and evaluation of motion quality after arthrodesis. Spine. 2013; 38(10):E594–601. [PubMed: 23429677]

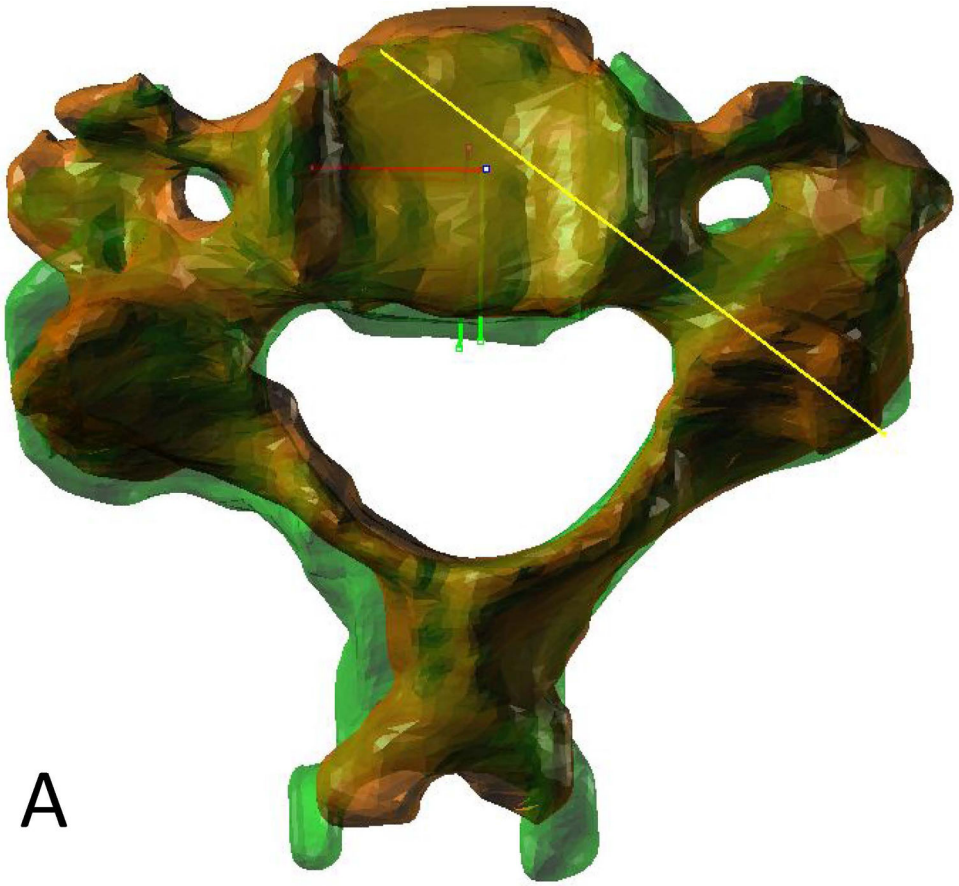

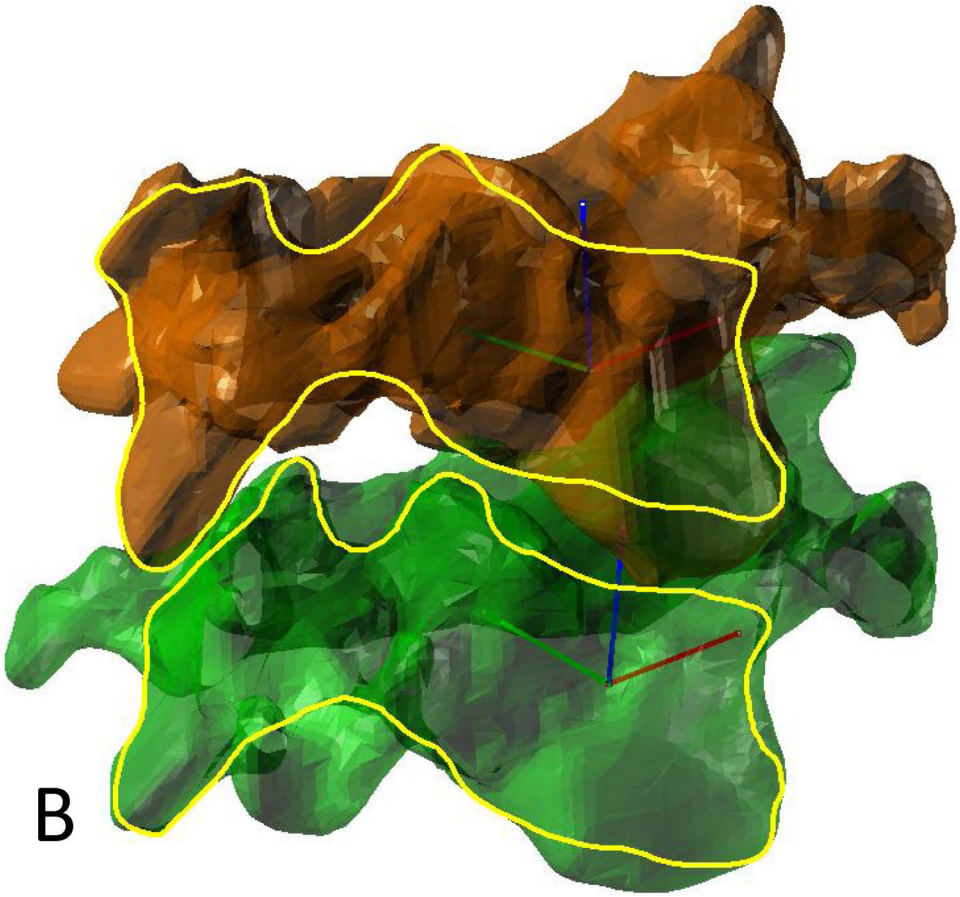

Figure 1.

A. By changing the point of view, the upper and lower pedicles on the right side of the neuroforamen at C3/C4 were adjusted to overlap completely. The central line along the long axis of the pedicles was defined on this plane. The pedicles were then cut along the central line perpendicular to this plane using Section tool.

B. The oblique sagittal plane passing through the long axis of both pedicles which composed the right side of the neuroforamen at C3/C4 was set up.

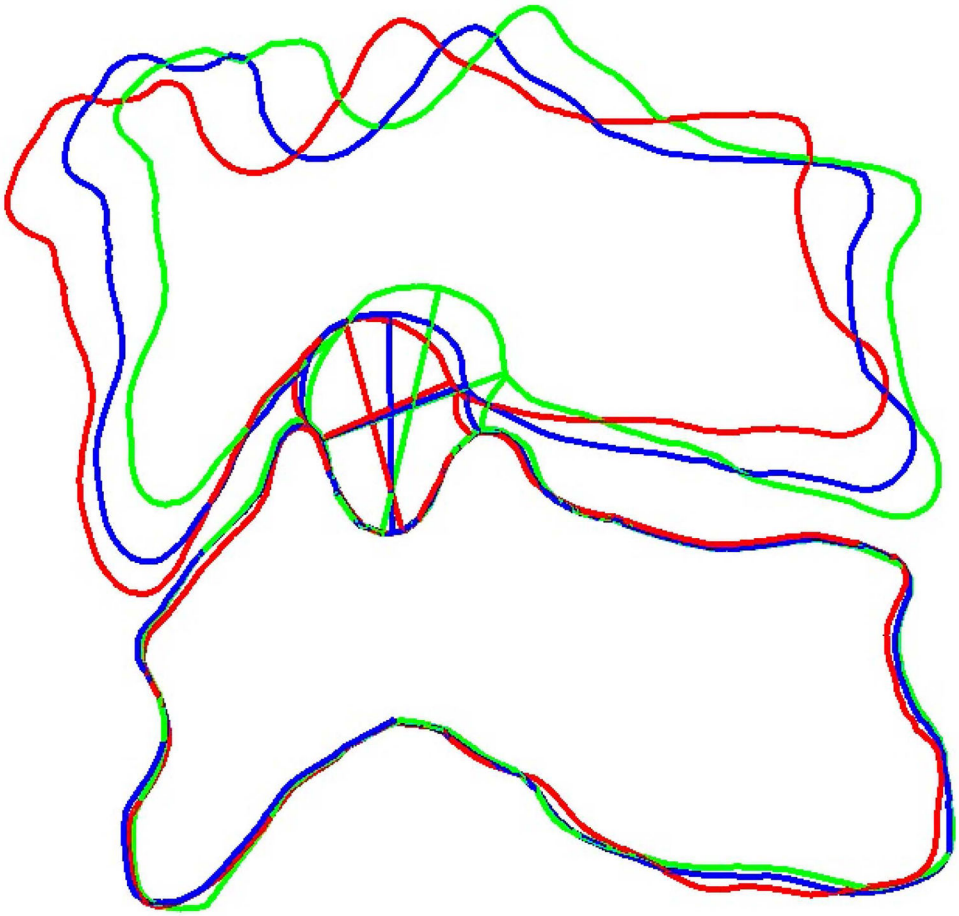

Figure 2.

The sagittal planes of C3/C4 in 3 positions (blue line: neutral; green line: flexion; red line: extension) were realigned on the same plane according to the superior edge of the lower pedicle. The dimensional changes (area, height and width) of the neuroforamen were well documented.

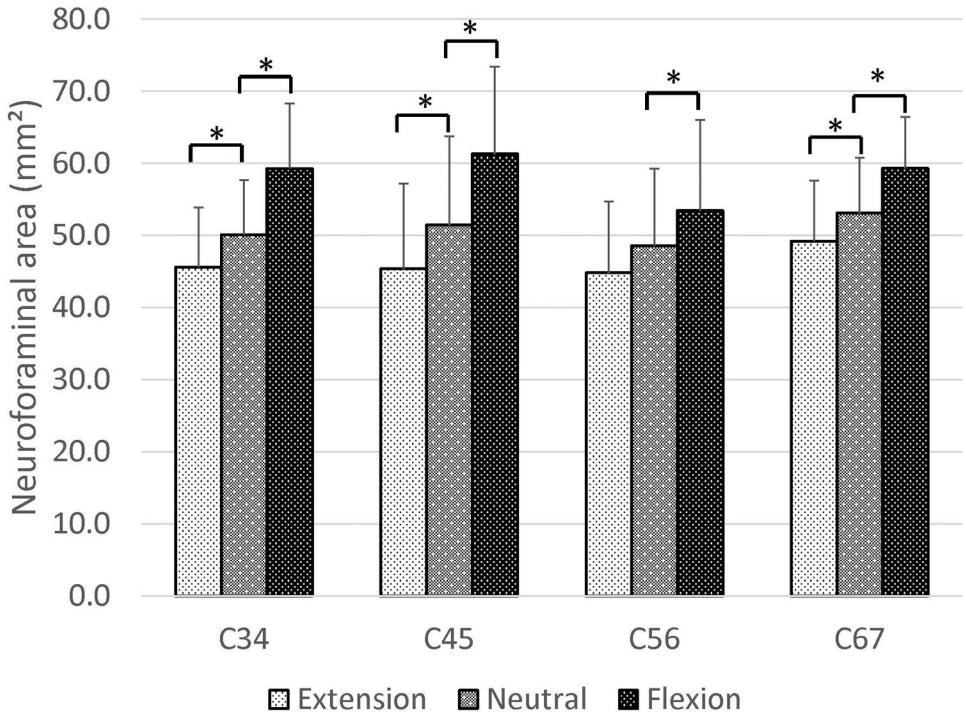

Figure 3.

Neuroforaminal area of the 4 segments in 3 positions during dynamic flexion-extension. * There were significant differences between the neutral position and flexion or extension (P<0.05). Error bars represent the standard deviations.

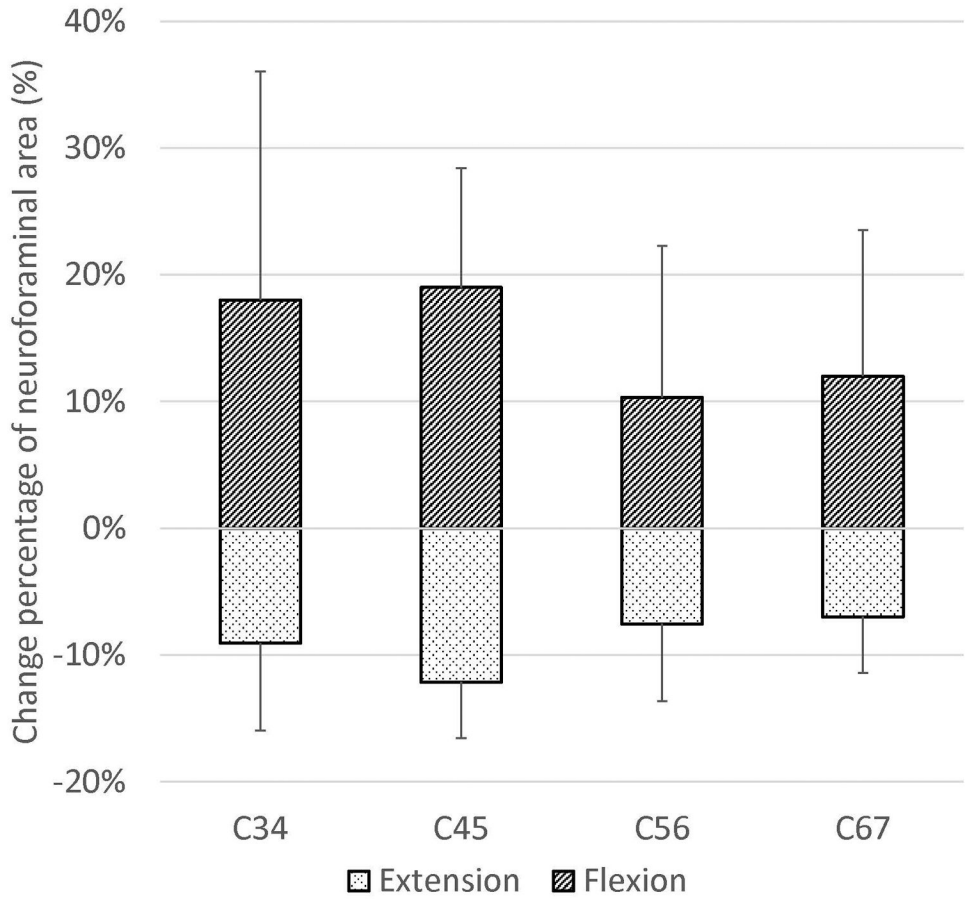

Figure 4.

The change percentage of the neuroforaminal area of the 4 segments in flexion and extension, compared with the neuroforaminal area in the neutral position. Error bars represent the standard deviations.

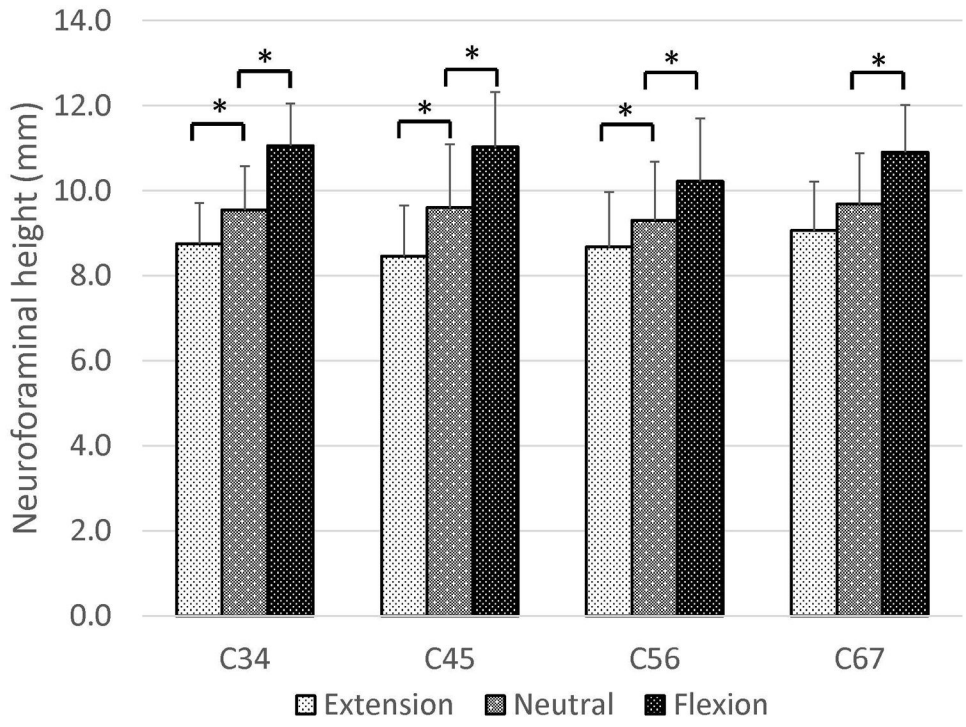

Figure 5.

Neuroforaminal height of the 4 segments in 3 positions during dynamic flexion-extension. * There were significant differences between the neutral position and flexion or extension (P<0.05). Error bars represent the standard deviations.

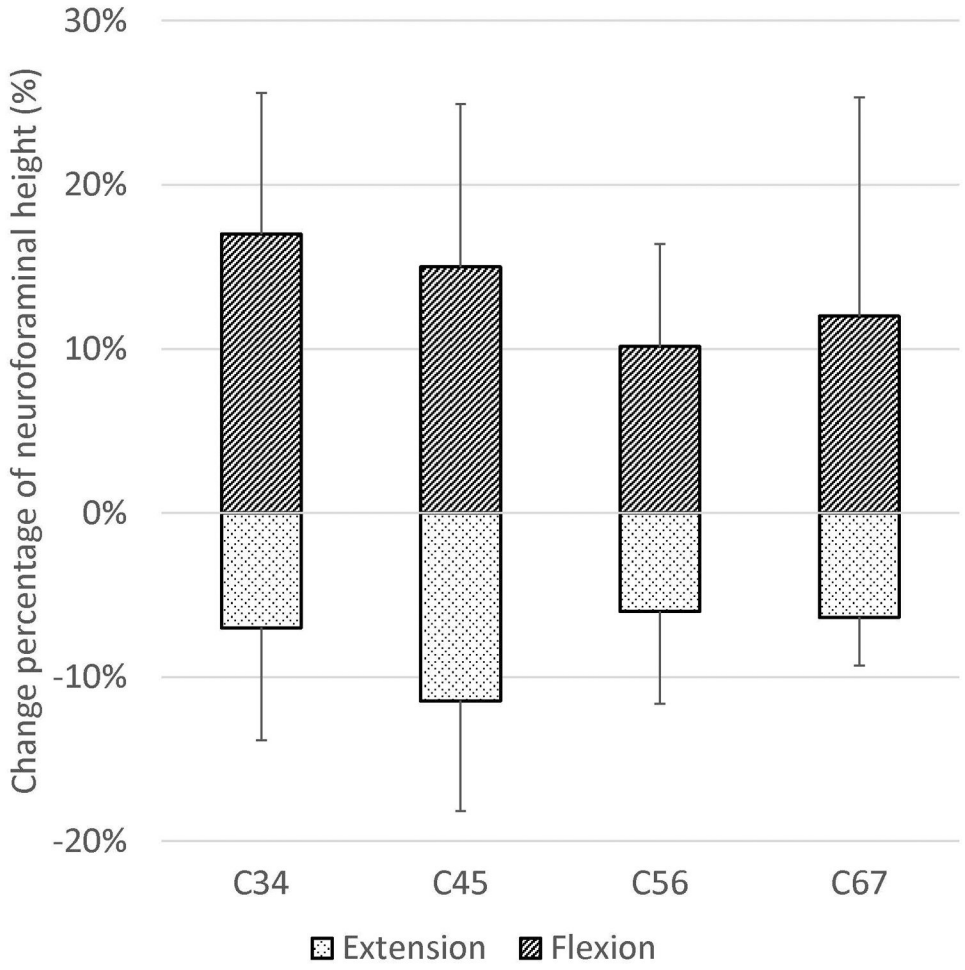

Figure 6.

The change percentage of the neuroforaminal height of the 4 segments in flexion and extension, compared with the neuroforaminal height in the neutral position. Error bars represent the standard deviations.

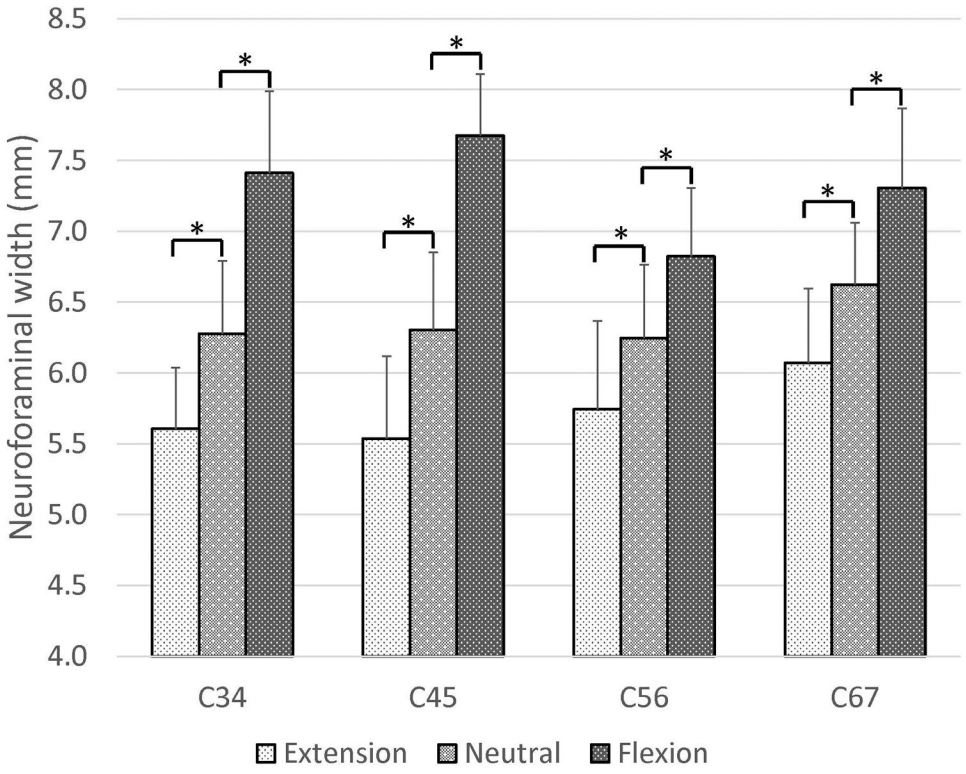

Figure 7.

Neuroforaminal width of the 4 segments in 3 positions during dynamic flexion-extension. * There were significant differences between the neutral position and flexion or extension (P<0.05). Error bars represent the standard deviations.

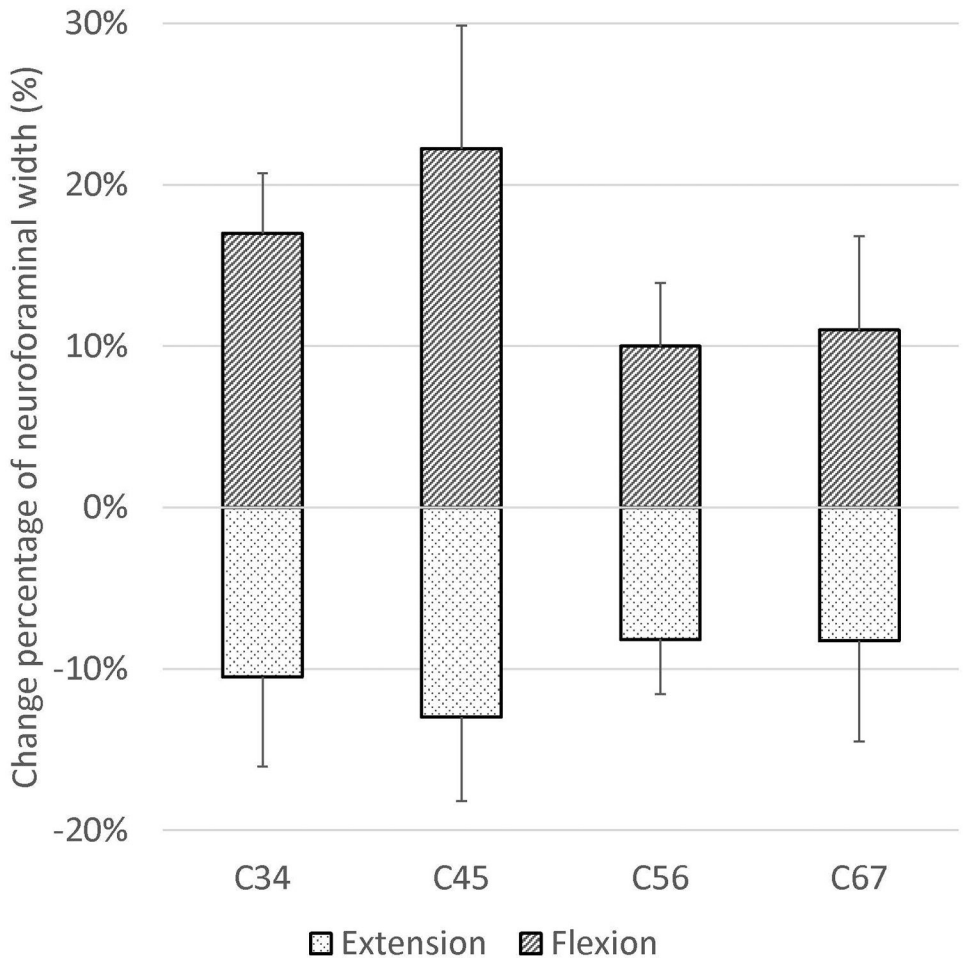

Figure 8.

The change percentage of the neuroforaminal width of the 4 segments in flexion and extension, compared with the neuroforaminal width in the neutral position. Error bars represent the standard deviations.